

ปรากฏการณ์ระจกเงาแม่เหล็กในการเคลื่อนที่ของอนุภาคพลังงานสูง
ในบริเวณที่มีการอัดตัวของพลาสมา

นายกิตติพัฒน์ มาลากิจ

ศูนย์วิจัยทรัพยากร

จุฬาลงกรณ์มหาวิทยาลัย

วิทยานิพนธ์นี้เป็นส่วนหนึ่งของการศึกษาตามหลักสูตรปริญญาวิทยาศาสตรมหาบัณฑิต

สาขาวิชาฟิสิกส์ ภาควิชาฟิสิกส์

คณะวิทยาศาสตร์ จุฬาลงกรณ์มหาวิทยาลัย

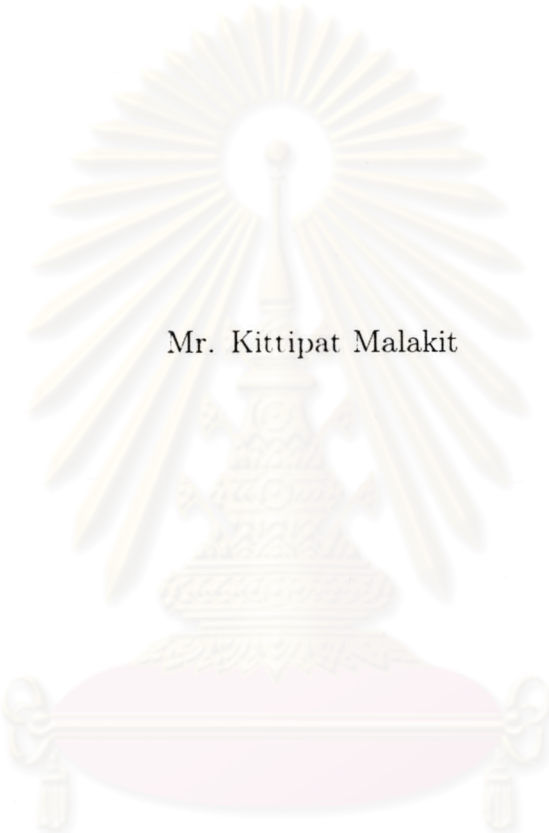
ปีการศึกษา 2545

ISBN 974-17-2491-8

ลิขสิทธิ์ของจุฬาลงกรณ์มหาวิทยาลัย

I21044041

MAGNETIC MIRRORING EFFECT ON THE MOTION OF
ENERGETIC PARTICLES IN PLASMA COMPRESSIONS



Mr. Kittipat Malakit

A Thesis Submitted in Partial Fulfillment of the Requirements
for the Degree of Master of Science in Physics

Department of Physics
Faculty of Science

Chulalongkorn University

Academic Year 2002

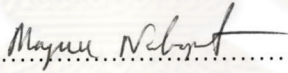
ISBN 974-17-2491-8

Thesis Title MAGNETIC MIRRORING EFFECT ON THE MOTION OF
ENERGETIC PARTICLES IN PLASMA COMPRESSIONS
By Mr. KITTIPAT MALAKIT
Field of Study Physics
Thesis Advisor Associate Professor David Ruffolo, Ph.D.


Accepted by the Faculty of Science, Chulalongkorn University in Partial
Fulfillment of the Requirements for the Master's Degree


..... Dean of Faculty of Science
(Associate Professor Wanchai Phothiphichitr, Ph.D.)

THESIS COMMITTEE

..... Chairman
(Associate Professor Mayuree Natenapit, Ph.D.)

..... Thesis Advisor
(Associate Professor David Ruffolo, Ph.D.)

..... Member
(Assistant Professor Udomsilp Pinsook, Ph.D.)

..... Member
(Rattachat Mongkolnavin, Ph.D.)

นาย กิตติพัฒน์ มาลากิจ : ปรากฏการณ์กระจกเงาแม่เหล็กในการเคลื่อนที่ของอนุภาคพลังงานสูงในบริเวณที่มีการอัดตัวของพลาสมา (MAGNETIC MIRRORING EFFECT ON THE MOTION OF ENERGETIC PARTICLES IN PLASMA COMPRESSIONS) อ. ที่ปรึกษา : รศ. ดร. เดวิด รุฟโฟโล, 159 หน้า. ISBN 974-17-2491-8.

เป็นที่เชื่อกันโดยทั่วไปว่าอนุภาครังสีคอสมิกถูกเร่งให้มีพลังงานสูงขึ้นได้ที่คลื่นกระแทกในอวกาศ ในการศึกษากลไกการเร่งนี้โดยส่วนมากจะใช้สมการการฟุ้งการพา (diffusion-convection equation) อย่างไรก็ตามสมการนี้เป็นสมการที่ถูกประมาณมาจากสมการการขนส่งแบบมุมซั้ว (pitch-angle transport equation) บนพื้นฐานของการประมาณการฟุ้ง (diffusion approximation) การเข้าสู่ปัญหาโดยใช้การขนส่งแบบมุมซั้วจะแม่นยำกว่าแต่จะซับซ้อนกว่า ในงานนี้เราได้ทำการจำลองการขนส่งของอนุภาคที่บริเวณที่มีการอัดตัวของพลาสมา ด้วยความกว้างของการอัดหลายๆ ค่า และบริเวณคลื่นกระแทก (ความกว้างของการอัดเป็นศูนย์) โดยการแก้สมการการขนส่งแบบมุมซั้วด้วยวิธีไฟไนต์ดิฟเฟอเรนซ์ (finite difference method) และสมการการฟุ้งการพาซึ่งไม่ได้พิจารณาการเปลี่ยนแปลงเชิงระบบในมุมซั้วด้วยวิธีชู้ตติง (shooting method) และนอกจากนั้นเรายังได้ทำการปรับเปลี่ยนมุมสนามแม่เหล็ก (field angle) ซึ่งนิยามเป็นมุมระหว่างสนามแม่เหล็กกับแนวตั้งฉากของระนาบคลื่นกระแทก/ระนาบการอัดอีกด้วย ผลของการขนส่งมุมซั้วกับการประมาณเป็นการฟุ้งการพาจะถูกนำมาเปรียบเทียบ และวิเคราะห์เพื่อแสดงให้เห็นถึงผลกระทบของการเปลี่ยนแปลงเชิงระบบในมุมซั้ว เราสรุปว่าปรากฏการณ์กระจกเงาแม่เหล็ก (mirroring effect) ซึ่งเป็นปรากฏการณ์ที่เกิดขึ้นเมื่อมีการพิจารณามุมซั้วของอนุภาคเท่านั้น สามารถที่จะเพิ่มประสิทธิภาพของการเร่งให้สูงขึ้นในกรณีที่มีความกว้างของการอัดมีค่าน้อย นอกจากนั้นเรายังพบว่าข้อสมมุติที่ว่า $j \propto p^{-1}$ ทำให้สมการการฟุ้งการพาทำนายผลการเร่งผิดพลาดด้วยเพราะข้อสมมุตินี้ต้องการลักษณะการกระจายตัวตามระยะทางของอนุภาค $j(z)$ ที่ไม่ขึ้นกับโมเมนตัม ซึ่งจะ เป็นปัญหาโดยเฉพาะกรณีที่ความกว้างของการอัดมีค่ามาก

ภาควิชา ฟิสิกส์
สาขาวิชา ฟิสิกส์
ปีการศึกษา 2545

ลายมือชื่อนิติ.....

ลายมือชื่ออาจารย์ที่ปรึกษา.....

4372211323 : MAJOR PHYSICS

KEY WORDS: SHOCK / COMPRESSION REGION / ACCELERATION / TRANSPORT EQUATION / MIRRORING

KITTIPAT MALAKIT : MAGNETIC MIRRORING EFFECT ON THE MOTION OF

ENERGETIC PARTICLES IN PLASMA COMPRESSIONS THESIS ADVISOR : ASSOC.

PROF. DAVID RUFFOLO, PhD., 159 pp. ISBN 974-17-2491-8.

It is commonly believed that most cosmic rays are accelerated at astrophysical shocks. Many works studying this acceleration mechanism have used a diffusion-convection equation (DC). Nevertheless, that is an approximate equation based on the diffusion approximation of a pitch-angle transport equation (PA). The PA approach is more precise and also more complicated. In this work, we simulate cosmic-ray particle transport at compression regions, with various compression widths, and shocks (zero width) by solving the PA equation with a finite-difference method and the DC equation, which does not take systematic pitch-angle changing into account, with a shooting method. Moreover, we also vary the field angle, defined as the angle between magnetic field lines and the normal to the shock/compression plane. The results from the PA and approximate DC approaches are compared and analyzed to point out the effects of systematic pitch-angle changes on the shock acceleration mechanism. We conclude that the magnetic mirroring effect, which appears only in the pitch-angle treatment, can enhance the acceleration mechanism in cases of narrow compression widths. Furthermore, found that the assumption of $j \propto p^{-\gamma}$ makes the DC equation yield incorrect acceleration efficiencies, because it requires the shape of the spatial distribution function, $j(z)$, to be independent of momentum, an assumption that is especially problematic in the case of a wide compression.

Department: Physics

Field of study: Physics

Academic year 2002

Student's signature.....*Kittipat Malakit*.....

Advisor's signature.....*David Ruffolo*.....

Acknowledgements

Foremost, I would really like to express my gratitude to my advisor, Assoc. Prof. Dr. David Ruffolo, very much for his treatment, guidance, and encouragement throughout the time I was his advisee. Apart from physics knowledge I have learnt from him, I have also developed myself a great deal, such as extending my vision, improving thinking skills, improving working skills, and developing English skills by both directly and indirectly learning from him.

I am also grateful to the thesis committee, Assoc. Prof. Dr. Mayuree Natenapit, Asst. Prof. Dr. Udomsilp Pinsook, and Dr. Rattachat Mongkolnavin, for reading and offering suggestions for this thesis.

Furthermore, I would like to thank Miss Thiranee Khumlumlert for providing me as much help and guidance as she could, Miss Kanokporn Leerungnavarat who gave me a lot of suggestions, especially when I was a beginner on the work of shock acceleration, Mr. Paisan Tooprakai for computer-system administration, Mr. Chanruangrit Channok for use of his personal computer in completing this work on time, Miss Kamonporn Klapping who helped and advised me a great deal on this thesis, Miss Suwicha Wannawichian who also offered many suggestions to me, and Miss Piyanate Chuychai for her discussion and help on using "IDL" and "Illustrator" software, which was very useful for this thesis.

Finally, I am extremely grateful to my father and my mother who are my inspiration and always support me to do good things. I am very proud to be their son and I hope to make them proud of me also; at least I have been trying.

This work was supported by the Thailand Research Fund.

Contents

Abstract in Thai.....	iv
Abstract in English.....	v
Acknowledgements.....	vi
Contents.....	vii
List of Figures.....	x
List of Tables.....	xxviii
Chapter 1 Introduction.....	1
1.1 Introduction.....	1
1.2 Objectives.....	3
1.3 Thesis Outline.....	3
Chapter 2 Background Knowledge.....	5
2.1 Cosmic Rays and Their Spectra and Origins.....	5
2.1.1 Cosmic Rays.....	5
2.1.2 Cosmic Ray Spectra and Origins.....	6
2.2 Magnetic Fields and Charged Particles in Space.....	15
2.2.1 A Charged Particle in a Magnetic Field.....	17
2.2.2 Magnetic Field in a Plasma.....	22
2.2.3 Cosmic Ray Motions in Space Plasmas.....	23
2.3 Shock Acceleration Concepts and Mechanism.....	25
2.3.1 Shocks.....	25
2.3.2 Shock Acceleration Mechanism.....	26
Chapter 3 Shock and Compression Models and Transport Equations.....	30
3.1 Shock and Compression Models.....	30
3.1.1 Shock Modelling.....	31

Contents (cont.)

3.1.2 Compression Region Modelling	32
3.2 Pitch-Angle Transport Equation	38
3.2.1 Pitch-Angle Distribution Function	38
3.2.2 General Form of the Pitch-Angle Transport Equation ...	40
3.2.3 Pitch-Angle Transport Equation for Cases of Interest ...	45
3.3 Diffusion-Convection Equation	50
Chapter 4 Transport Simulation	
Methodologies	56
4.1 Transport Simulation by Solving the Diffusion-Convection	
Equation	56
4.2 Transport Simulation by Solving the Pitch-Angle Transport	
Equation	59
4.2.1 Numerical Method of Solving the Pitch-Angle Transport	
Equation for a Compression Region	59
4.2.2 Orbit-Tracing Treatment for Shocks	67
4.2.3 Simulation Procedure	69
Chapter 5 Results and Discussion	75
5.1 Introduction to and Notes on Results	75
5.2 Results and Discussion	77
Chapter 6 Summary	86
References	88
Appendices	91
Appendix A $n(p)$ vs. $j(E)$ and γ vs. γ_E	92
Appendix B Origin of GCR: Supernova Shocks	95
Appendix C Simulation Parameters	97

Appendix D All Results 101
Vitae 159



ศูนย์วิทยทรัพยากร
จุฬาลงกรณ์มหาวิทยาลัย

List of Figures

Figure	Page
Figure 2.1	Energy spectra of various cosmic ray species in the energy range above 10^7 eV (Picture credit: Simpson 1983) 7
Figure 2.2	All-cosmic-ray-particle spectrum at high energy with different spectral indices for different energy ranges (the flux is scaled by $E^{2.5}$ to see the slope differences more easily) (Picture credit: http://www.phys.washington.edu/~walta) 9
Figure 2.3	A supernova remnant, which looks like an expanding bubble with shock waves around the outer rim. (Picture credit: http://www.astro.columbia.edu/~ben)..... 10
Figure 2.4	Time-integrated intensities of oxygen from ≈ 300 eV/nucleon to ≈ 300 MeV/nucleon (Picture credit: Mewaldt et al. 2001) 12
Figure 2.5	Time-integrated intensities of helium, oxygen, and iron from ≈ 300 eV/nucleon to ≈ 300 MeV/nucleon (Picture credit: Mewaldt et al. 2001) 13
Figure 2.6	A shock due to a CME (Picture credit: Cravens 1997)..... 14
Figure 2.7	A shock at a CIR (Picture credit: Hundhausen 1972)..... 15
Figure 2.8	The solar wind termination shock and anomalous cosmic rays ACRs. (Picture credit: http://helios.gsfc.nasa.gov) 16
Figure 2.9	Helical motion of a charged particle in a uniform magnetic field 18
Figure 2.10	Side view of the helical motion, indicating the pitch angle 18

List of Figures (cont.)

- Figure 2.11 Helical motion of particles in a uniform magnetic field with various pitch angles..... 19
- Figure 2.12 Motion of a particle in a converging magnetic field (a) and magnetic mirroring in the Earth's radiation belts (b) (Picture credit: Jackson 1975 and <http://www.estec.esa.nl/wmwww/WMA/backgnd.html>).....21
- Figure 2.13 A charged particle changes its pitch angle along an irregular magnetic field. Furthermore, the direction of motion of the charged particle can also change. 22
- Figure 2.14 The motion of a cosmic ray along a magnetic field line frozen in the solar wind. (Picture credit: Chuychai et al. 2003) 24
- Figure 2.15 A shock, here produced by a bullet, divides a fluid into two regions, upstream and downstream. Fluid properties of the two regions are quite different, and change sharply at the shock... 26
- Figure 2.16 A head-on collision and a following collision between a particle of small mass and an obstacle of large mass.....28
- Figure 2.17 A demonstration of shock acceleration 29
- Figure 3.1 Our model of an astrophysical shock; $\hat{\mathbf{l}}$ is a unit vector in the direction of the magnetic field line, \mathbf{U} is the plasma velocity, $\hat{\mathbf{n}}$ is the shock normal vector, and θ is the field angle. The subscripts "1" and "2" are labels for upstream and downstream, respectively.....31

List of Figures (cont.)

- Figure 3.2 Magnetic field configuration model comparison between the “kink” configuration of a shock and hyperbolic configuration of a compression region. The half-conjugate axis, b , is used to parameterize the width of the compression..... 33
- Figure 3.3 A hyperbolic function in the primed coordinates with center at (h, k) ; $2a$ is the length of the major axis, $2b$ is the length of the conjugate axis, $2c$ is the length between the two foci..... 34
- Figure 3.4 A shifted hyperbolic function in primed coordinates, following equation (3.2), in the view point of unprimed coordinates. $\theta = (\theta_2 + \theta_1)/2$ is the angle between the primed axes and unprimed axes (rotation angle) and $\theta_h = (\theta_2 - \theta_1)/2$ is the angle between the asymptotic lines and the z' axis, where θ_1 and θ_2 are angles between the upper asymptotic lines and the z axis upstream and downstream, respectively..... 35
- Figure 3.5 The structure of our compression region model in the normal incidence frame, where plasma flows to encounter the compression plane in the direction normal to the plane. Plasma speed and magnetic intensity are changed in only z direction. $\hat{\mathbf{l}}$ is the unit vector in the direction of magnetic field, \mathbf{U} is the plasma velocity, $\hat{\mathbf{n}}$ is compression plane normal vector..... 37
- Figure 3.6 Schematic showing a distribution volume in our pitch-angle transport space..... 39
- Figure 3.7 (a) Systematic process leading to convective flux. (b) Random process leading to diffusive flux..... 41

List of Figures (cont.)

- Figure 3.8 Fluxes move through a given volume in the z , p , and μ directions; if the incoming S does not balance the outgoing S , the particle number in the volume changes..... 42
- Figure 3.9 The pitch-angle scattering making particles undergo a random walk in μ , represented by up-down arrows, while the streaming process makes particles move along z with velocity $v_z \approx \mu v$, represented by horizontal arrows with μ -dependent magnitudes. (Picture credit: Klappong M.Sc. Thesis 2002)..... 51
- Figure 3.10 Demonstration of diffusion of anisotropic particles in the z -direction due to the effect of the pitch-angle scattering and the μ -dependent streaming. Left panels: density plots of particles in the μ - z plane. Right panels: particle density F vs. z 52
- Figure 4.1 The interpolation scheme. The solid lines are at constant t . The dashes lines are characteristics, along which pF is constant. The value of $F(t_{i+1}, p_w)$ can be found from $F(t_i, p^*)$, which can be estimated by geometric interpolation between $F(t_i, p_{w-1})$ and $F(t_i, p_w)$ 63
- Figure 4.2 The particle helical orbit path near an oblique shock, along with the relevant definitions of coordinates (Picture credit: Leerungnavarat et al. (2000), adapted from Teresawa (1979))..... 68
- Figure 4.3 (a) An acceptable numerical ΔF over a short time Δt , compared with (b) an analytical ΔF 71
- Figure 4.4 (a) An unacceptable numerical ΔF over a short time Δt , compared with (b) an analytical ΔF 72

List of Figures (cont.)

- Figure 4.5 Schematic illustration of the balanced fluxes at shock in steady state (Picture credit: Ruffolo 1999).....73
- Figure 5.1 Two graphs of $\log j$ vs. $\log p$ with two different γ values: $-\gamma$ is the slope of the graph, used to indicate acceleration efficiency at the momentum of interest, p_0 . For the same particle density at p_0 , a higher γ at p_0 gives a smaller particle number density at a higher momentum, p_1 ; a lower γ at p_0 gives a greater particle number density at a higher momentum, p_1 . Therefore, a lower γ implies a greater acceleration efficiency. 76
- Figure 5.2 Steady state spatial density of particles with an energy corresponding with $v/U_{1n} = 25$ in the cases of shocks, obtained from solving the pitch-angle transport equation. The jump height is highest in the quasi-perpendicular case (Q-Perp; solid line), lower in the oblique case (OB; dashed line), and disappears in the quasi-parallel case (Q-Par; dotted line). 77
- Figure 5.3 Steady state spatial density of particles with an energy corresponding with $v/U_{1n} = 25$ in the cases of a quasi-perpendicular shock (solid line), compression region with $b/\lambda_{\parallel} = 0.2$ (dashed line), and compression region with $b/\lambda_{\parallel} = 0.5$ (dotted line), obtained from solving the pitch-angle transport equation 78

List of Figures (cont.)

- Figure 5.4 Steady state spatial density of particles with an energy corresponding with $v/U_{1n} = 25$ in the case of a quasi-parallel compression region with $b/\lambda_{\parallel} = 0.2$, obtained from solving the pitch-angle transport equation (PA; solid line) and diffusion-convection equation (DC; dotted line)..... 79
- Figure 5.5 Particle spectra of quasi-perpendicular (Q-Perp; solid line), oblique (OB; dashed line) and quasi-parallel (Q-Par; dotted line) shocks, obtained by the pitch-angle transport equation. Here, they are normalized to one at the momentum corresponding with $v/U_{1n} = 25$ 80
- Figure 5.6 Spectral index, γ , of particles with an energy corresponding with $v/U_{1n} = 25$ versus width of compression (shock \equiv zero width compression region) in the cases of quasi-perpendicular shock/compression regions, obtained from solving the pitch-angle transport equation (PA; solid line) and diffusion-convection equation (DC; dotted line)..... 80
- Figure 5.7 Spectral index, γ , of particles with an energy corresponding with $v/U_{1n} = 25$ versus width of compression (shock \equiv zero width compression region) in the cases of quasi-parallel shock/compression regions, obtained from solving the pitch-angle transport equation (PA; solid line) and diffusion-convection equation (DC; dotted line)..... 81

List of Figures (cont.)

- Figure 5.8 Steady state spatial density of particles with an energy corresponding with (a) $v/U_{1n} = 25$ and (b) $v/U_{1n} = 50$ in the case of a quasi-perpendicular compression region with $b/\lambda_{\parallel} = 2.0$, obtained from solving the pitch-angle transport equation (PA; solid line) and diffusion-convection equation (DC; dotted line)..... 82
- Figure 5.9 Steady state spatial density of particles with an energy corresponding with (a) $v/U_{1n} = 25$ and (b) $v/U_{1n} = 50$ in the case of a quasi-parallel compression region with $b/\lambda_{\parallel} = 0.2$, obtained from solving the pitch-angle transport equation (PA; solid line) and diffusion-convection equation (DC; dotted line)..... 83
- Figure 5.10 Steady state spatial density of particles with an energy corresponding with $v/U_{1n} = 50$ in the case of a quasi-parallel compression region with $b/\lambda_{\parallel} = 0.2$, obtained from solving the pitch-angle transport equation (PA; solid line) and diffusion-convection equation (DC; dotted line)..... 84
- Figure 5.11 Spectral index, γ , of particles with an energy corresponding with $v/U_{1n} = 50$ versus width of compression (shock \equiv zero width compression region) in the cases of quasi-perpendicular shock/compression regions, obtained from solving the pitch-angle transport equation (PA; solid line) and diffusion-convection equation (DC; dotted line)..... 84

List of Figures (cont.)

Figure 5.12	Spectral index, γ , of particles with an energy corresponding with $v/U_{1n} = 50$ versus width of compression (shock \equiv zero width compression region) in the cases of quasi-parallel shock/compression regions, obtained from solving the pitch-angle transport equation (PA; solid line) and diffusion-convection equation (DC; dotted line).....	85
Figure D.1	$\langle j \rangle_\mu$ vs. z/λ_\parallel of a quasi-perpendicular shock, $v/U_{1n}=25$	102
Figure D.2	$\langle j \rangle_\mu$ vs. z/λ_\parallel of a quasi-perpendicular shock, $v/U_{1n}=50$	102
Figure D.3	$\langle j \rangle_\mu$ vs. z/λ_\parallel of a quasi-perpendicular compression region with $b/\lambda_\parallel = 0.2$, $v/U_{1n}=25$	103
Figure D.4	$\langle j \rangle_\mu$ vs. z/λ_\parallel of a quasi-perpendicular compression region with $b/\lambda_\parallel = 0.2$, $v/U_{1n}=50$	103
Figure D.5	$\langle j \rangle_\mu$ vs. z/λ_\parallel of a quasi-perpendicular compression region with $b/\lambda_\parallel = 0.5$, $v/U_{1n}=25$	104
Figure D.6	$\langle j \rangle_\mu$ vs. z/λ_\parallel of a quasi-perpendicular compression region with $b/\lambda_\parallel = 0.5$, $v/U_{1n}=50$	104
Figure D.7	$\langle j \rangle_\mu$ vs. z/λ_\parallel of a quasi-perpendicular compression region with $b/\lambda_\parallel = 1.0$, $v/U_{1n}=25$	105
Figure D.8	$\langle j \rangle_\mu$ vs. z/λ_\parallel of a quasi-perpendicular compression region with $b/\lambda_\parallel = 1.0$, $v/U_{1n}=50$	105
Figure D.9	$\langle j \rangle_\mu$ vs. z/λ_\parallel of a quasi-perpendicular compression region with $b/\lambda_\parallel = 2.0$, $v/U_{1n}=25$	106

List of Figures (cont.)

Figure D.10	$\langle j \rangle_\mu$ vs. z/λ_\parallel of a quasi-perpendicular compression region with $b/\lambda_\parallel = 2.0$, $v/U_{1n}=50$	106
Figure D.11	$\langle j \rangle_\mu$ vs. z/λ_\parallel of an oblique shock, $v/U_{1n}=25$	107
Figure D.12	$\langle j \rangle_\mu$ vs. z/λ_\parallel of an oblique shock, $v/U_{1n}=50$	107
Figure D.13	$\langle j \rangle_\mu$ vs. z/λ_\parallel of an oblique compression region with $b/\lambda_\parallel = 0.2$, $v/U_{1n}=25$	108
Figure D.14	$\langle j \rangle_\mu$ vs. z/λ_\parallel of an oblique compression region with $b/\lambda_\parallel = 0.2$, $v/U_{1n}=50$	108
Figure D.15	$\langle j \rangle_\mu$ vs. z/λ_\parallel of an oblique compression region with $b/\lambda_\parallel = 0.5$, $v/U_{1n}=25$	109
Figure D.16	$\langle j \rangle_\mu$ vs. z/λ_\parallel of an oblique compression region with $b/\lambda_\parallel = 0.5$, $v/U_{1n}=50$	109
Figure D.17	$\langle j \rangle_\mu$ vs. z/λ_\parallel of an oblique compression region with $b/\lambda_\parallel = 1.0$, $v/U_{1n}=25$	110
Figure D.18	$\langle j \rangle_\mu$ vs. z/λ_\parallel of an oblique compression region with $b/\lambda_\parallel = 1.0$, $v/U_{1n}=50$	110
Figure D.19	$\langle j \rangle_\mu$ vs. z/λ_\parallel of an oblique compression region with $b/\lambda_\parallel = 2.0$, $v/U_{1n}=25$	111
Figure D.20	$\langle j \rangle_\mu$ vs. z/λ_\parallel of an oblique compression region with $b/\lambda_\parallel = 2.0$, $v/U_{1n}=50$	111
Figure D.21	$\langle j \rangle_\mu$ vs. z/λ_\parallel of a quasi-parallel shock, $v/U_{1n}=25$	112
Figure D.22	$\langle j \rangle_\mu$ vs. z/λ_\parallel of a quasi-parallel shock, $v/U_{1n}=50$	112

List of Figures (cont.)

Figure D.23	$\langle j \rangle_\mu$ vs. z/λ_\parallel of a quasi-parallel compression region with $b/\lambda_\parallel = 0.2$, $v/U_{1n}=25$	113
Figure D.24	$\langle j \rangle_\mu$ vs. z/λ_\parallel of a quasi-parallel compression region with $b/\lambda_\parallel = 0.2$, $v/U_{1n}=50$	113
Figure D.25	$\langle j \rangle_\mu$ vs. z/λ_\parallel of a quasi-parallel compression region with $b/\lambda_\parallel = 0.5$, $v/U_{1n}=25$	114
Figure D.26	$\langle j \rangle_\mu$ vs. z/λ_\parallel of a quasi-parallel compression region with $b/\lambda_\parallel = 0.5$, $v/U_{1n}=50$	114
Figure D.27	$\langle j \rangle_\mu$ vs. z/λ_\parallel of a quasi-parallel compression region with $b/\lambda_\parallel = 1.0$, $v/U_{1n}=25$	115
Figure D.28	$\langle j \rangle_\mu$ vs. z/λ_\parallel of a quasi-parallel compression region with $b/\lambda_\parallel = 1.0$, $v/U_{1n}=50$	115
Figure D.29	$\langle j \rangle_\mu$ vs. z/λ_\parallel of a quasi-parallel compression region with $b/\lambda_\parallel = 2.0$, $v/U_{1n}=25$	116
Figure D.30	$\langle j \rangle_\mu$ vs. z/λ_\parallel of a quasi-parallel compression region with $b/\lambda_\parallel = 2.0$, $v/U_{1n}=50$	116
Figure D.31	$\log\langle j \rangle_1$ vs. $\log(p)$ of a quasi-perpendicular shock obtained by the pitch-angle transport equation	117
Figure D.32	$\log\langle j \rangle_1$ vs. $\log(p)$ of a quasi-perpendicular compression region with $b/\lambda_\parallel = 0.2$ obtained by the pitch-angle transport equation	117

List of Figures (cont.)

- Figure D.33 $\log\langle j \rangle_1$ vs. $\log(p)$ of a quasi-perpendicular compression region with $b/\lambda_{\parallel} = 0.5$ obtained by the pitch-angle transport equation 118
- Figure D.34 $\log\langle j \rangle_1$ vs. $\log(p)$ of a quasi-perpendicular compression region with $b/\lambda_{\parallel} = 1.0$ obtained by the pitch-angle transport equation 118
- Figure D.35 $\log\langle j \rangle_1$ vs. $\log(p)$ of a quasi-perpendicular compression region with $b/\lambda_{\parallel} = 2.0$ obtained by the pitch-angle transport equation 119
- Figure D.36 $\log\langle j \rangle_1$ vs. $\log(p)$ of an oblique shock obtained by the pitch-angle transport equation 119
- Figure D.37 $\log\langle j \rangle_1$ vs. $\log(p)$ of an oblique compression region with $b/\lambda_{\parallel} = 0.2$ obtained by the pitch-angle transport equation 120
- Figure D.38 $\log\langle j \rangle_1$ vs. $\log(p)$ of an oblique compression region with $b/\lambda_{\parallel} = 0.5$ obtained by the pitch-angle transport equation 120
- Figure D.39 $\log\langle j \rangle_1$ vs. $\log(p)$ of an oblique compression region with $b/\lambda_{\parallel} = 1.0$ obtained by the pitch-angle transport equation 121
- Figure D.40 $\log\langle j \rangle_1$ vs. $\log(p)$ of an oblique compression region with $b/\lambda_{\parallel} = 2.0$ obtained by the pitch-angle transport equation 121
- Figure D.41 $\log\langle j \rangle_1$ vs. $\log(p)$ of a quasi-parallel shock obtained by the pitch-angle transport equation 122
- Figure D.42 $\log\langle j \rangle_1$ vs. $\log(p)$ of a quasi-parallel compression region with $b/\lambda_{\parallel} = 0.2$ obtained by the pitch-angle transport equation ... 122

List of Figures (cont.)

- Figure D.43 $\log\langle j \rangle_1$ vs. $\log(p)$ of a quasi-parallel compression region with $b/\lambda_{\parallel} = 0.5$ obtained by the pitch-angle transport equation... 123
- Figure D.44 $\log\langle j \rangle_1$ vs. $\log(p)$ of a quasi-parallel compression region with $b/\lambda_{\parallel} = 1.0$ obtained by the pitch-angle transport equation... 123
- Figure D.45 $\log\langle j \rangle_1$ vs. $\log(p)$ of a quasi-parallel compression region with $b/\lambda_{\parallel} = 2.0$ obtained by the pitch-angle transport equation... 124
- Figure D.46 Spectral index, γ , of particles with an energy corresponding with $v/U_{1n} = 25$ versus width of compression (shock \equiv zero width compression region) in the cases of quasi-perpendicular shock/compression regions, obtained from solving the pitch-angle transport equation (PA; solid line) and diffusion-convection equation (DC; dotted line).....126
- Figure D.47 Spectral index, γ , of particles with an energy corresponding with $v/U_{1n} = 50$ versus width of compression (shock \equiv zero width compression region) in the cases of quasi-perpendicular shock/compression regions, obtained from solving the pitch-angle transport equation (PA; solid line) and diffusion-convection equation (DC; dotted line).....126
- Figure D.48 Spectral index, γ , of particles with an energy corresponding with $v/U_{1n} = 25$ versus width of compression (shock \equiv zero width compression region) in the cases of oblique shock/compression regions, obtained from solving the pitch-angle transport equation (PA; solid line) and diffusion-convection equation (DC; dotted line). 127

List of Figures (cont.)

- Figure D.49 Spectral index, γ , of particles with an energy corresponding with $v/U_{1n} = 50$ versus width of compression (shock \equiv zero width compression region) in the cases of oblique shock/compression regions, obtained from solving the pitch-angle transport equation (PA; solid line) and diffusion-convection equation (DC; dotted line). 127
- Figure D.50 Spectral index, γ , of particles with an energy corresponding with $v/U_{1n} = 25$ versus width of compression (shock \equiv zero width compression region) in the cases of quasi-parallel shock/compression regions, obtained from solving the pitch-angle transport equation (PA; solid line) and diffusion-convection equation (DC; dotted line). 128
- Figure D.51 Spectral index, γ , of particles with an energy corresponding with $v/U_{1n} = 50$ versus width of compression (shock \equiv zero width compression region) in the cases of quasi-parallel shock/compression regions, obtained from solving the pitch-angle transport equation (PA; solid line) and diffusion-convection equation (DC; dotted line). 128
- Figure D.52 $\ln\langle j \rangle_\mu$ vs. z/λ_\parallel of a quasi-perpendicular shock, $v/U_{1n}=25$. . . 129
- Figure D.53 $\ln\langle j \rangle_\mu$ vs. z/λ_\parallel of a quasi-perpendicular shock, $v/U_{1n}=50$. . . 129
- Figure D.54 $\ln\langle j \rangle_\mu$ vs. z/λ_\parallel of a quasi-perpendicular compression region with $b/\lambda_\parallel = 0.2$, $v/U_{1n}=25$ 130
- Figure D.55 $\ln\langle j \rangle_\mu$ vs. z/λ_\parallel of a quasi-perpendicular compression region with $b/\lambda_\parallel = 0.2$, $v/U_{1n}=50$ 130

List of Figures (cont.)

Figure D.56	$\ln\langle j \rangle_\mu$ vs. z/λ_\parallel of a quasi-perpendicular compression region with $b/\lambda_\parallel = 0.5$, $v/U_{1n}=25$	131
Figure D.57	$\ln\langle j \rangle_\mu$ vs. z/λ_\parallel of a quasi-perpendicular compression region with $b/\lambda_\parallel = 0.5$, $v/U_{1n}=50$	131
Figure D.58	$\ln\langle j \rangle_\mu$ vs. z/λ_\parallel of a quasi-perpendicular compression region with $b/\lambda_\parallel = 1.0$, $v/U_{1n}=25$	132
Figure D.59	$\ln\langle j \rangle_\mu$ vs. z/λ_\parallel of a quasi-perpendicular compression region with $b/\lambda_\parallel = 1.0$, $v/U_{1n}=50$	132
Figure D.60	$\ln\langle j \rangle_\mu$ vs. z/λ_\parallel of a quasi-perpendicular compression region with $b/\lambda_\parallel = 2.0$, $v/U_{1n}=25$	133
Figure D.61	$\ln\langle j \rangle_\mu$ vs. z/λ_\parallel of a quasi-perpendicular compression region with $b/\lambda_\parallel = 2.0$, $v/U_{1n}=50$	133
Figure D.62	$\ln\langle j \rangle_\mu$ vs. z/λ_\parallel of an oblique shock, $v/U_{1n}=25$	134
Figure D.63	$\ln\langle j \rangle_\mu$ vs. z/λ_\parallel of an oblique shock, $v/U_{1n}=50$	134
Figure D.64	$\ln\langle j \rangle_\mu$ vs. z/λ_\parallel of an oblique compression region with $b/\lambda_\parallel = 0.2$, $v/U_{1n}=25$	135
Figure D.65	$\ln\langle j \rangle_\mu$ vs. z/λ_\parallel of an oblique compression region with $b/\lambda_\parallel = 0.2$, $v/U_{1n}=50$	135
Figure D.66	$\ln\langle j \rangle_\mu$ vs. z/λ_\parallel of an oblique compression region with $b/\lambda_\parallel = 0.5$, $v/U_{1n}=25$	136
Figure D.67	$\ln\langle j \rangle_\mu$ vs. z/λ_\parallel of an oblique compression region with $b/\lambda_\parallel = 0.5$, $v/U_{1n}=50$	136

List of Figures (cont.)

Figure D.68	$\ln\langle j \rangle_\mu$ vs. z/λ_\parallel of an oblique compression region with $b/\lambda_\parallel = 1.0$, $v/U_{1n}=25$	137
Figure D.69	$\ln\langle j \rangle_\mu$ vs. z/λ_\parallel of an oblique compression region with $b/\lambda_\parallel = 1.0$, $v/U_{1n}=50$	137
Figure D.70	$\ln\langle j \rangle_\mu$ vs. z/λ_\parallel of an oblique compression region with $b/\lambda_\parallel = 2.0$, $v/U_{1n}=25$	138
Figure D.71	$\ln\langle j \rangle_\mu$ vs. z/λ_\parallel of an oblique compression region with $b/\lambda_\parallel = 2.0$, $v/U_{1n}=50$	138
Figure D.72	$\ln\langle j \rangle_\mu$ vs. z/λ_\parallel of a quasi-parallel shock, $v/U_{1n}=25$	139
Figure D.73	$\ln\langle j \rangle_\mu$ vs. z/λ_\parallel of a quasi-parallel shock, $v/U_{1n}=50$	139
Figure D.74	$\ln\langle j \rangle_\mu$ vs. z/λ_\parallel of a quasi-parallel compression region with $b/\lambda_\parallel =$ 0.2 , $v/U_{1n}=25$	140
Figure D.75	$\ln\langle j \rangle_\mu$ vs. z/λ_\parallel of a quasi-parallel compression region with $b/\lambda_\parallel =$ 0.2 , $v/U_{1n}=50$	140
Figure D.76	$\ln\langle j \rangle_\mu$ vs. z/λ_\parallel of a quasi-parallel compression region with $b/\lambda_\parallel =$ 0.5 , $v/U_{1n}=25$	141
Figure D.77	$\ln\langle j \rangle_\mu$ vs. z/λ_\parallel of a quasi-parallel compression region with $b/\lambda_\parallel =$ 0.5 , $v/U_{1n}=50$	141
Figure D.78	$\ln\langle j \rangle_\mu$ vs. z/λ_\parallel of a quasi-parallel compression region with $b/\lambda_\parallel =$ 1.0 , $v/U_{1n}=25$	142
Figure D.79	$\ln\langle j \rangle_\mu$ vs. z/λ_\parallel of a quasi-parallel compression region with $b/\lambda_\parallel =$ 1.0 , $v/U_{1n}=50$	142

List of Figures (cont.)

Figure D.80	$\ln\langle j \rangle_\mu$ vs. z/λ_{\parallel} of a quasi-parallel compression region with $b/\lambda_{\parallel} = 2.0$, $v/U_{1n}=25$	143
Figure D.81	$\ln\langle j \rangle_\mu$ vs. z/λ_{\parallel} of a quasi-parallel compression region with $b/\lambda_{\parallel} = 2.0$, $v/U_{1n}=50$	143
Figure D.82	δ vs. z/λ_{\parallel} of a quasi-perpendicular shock, $v/U_{1n}=25$	144
Figure D.83	δ vs. z/λ_{\parallel} of a quasi-perpendicular shock, $v/U_{1n}=50$	144
Figure D.84	δ vs. z/λ_{\parallel} of a quasi-perpendicular compression region with $b/\lambda_{\parallel} = 0.2$, $v/U_{1n}=25$	145
Figure D.85	δ vs. z/λ_{\parallel} of a quasi-perpendicular compression region with $b/\lambda_{\parallel} = 0.2$, $v/U_{1n}=50$	145
Figure D.86	δ vs. z/λ_{\parallel} of a quasi-perpendicular compression region with $b/\lambda_{\parallel} = 0.5$, $v/U_{1n}=25$	146
Figure D.87	δ vs. z/λ_{\parallel} of a quasi-perpendicular compression region with $b/\lambda_{\parallel} = 0.5$, $v/U_{1n}=50$	146
Figure D.88	δ vs. z/λ_{\parallel} of a quasi-perpendicular compression region with $b/\lambda_{\parallel} = 1.0$, $v/U_{1n}=25$	147
Figure D.89	δ vs. z/λ_{\parallel} of a quasi-perpendicular compression region with $b/\lambda_{\parallel} = 1.0$, $v/U_{1n}=50$	147
Figure D.90	δ vs. z/λ_{\parallel} of a quasi-perpendicular compression region with $b/\lambda_{\parallel} = 2.0$, $v/U_{1n}=25$	148
Figure D.91	δ vs. z/λ_{\parallel} of a quasi-perpendicular compression region with $b/\lambda_{\parallel} = 2.0$, $v/U_{1n}=50$	148
Figure D.92	δ vs. z/λ_{\parallel} of an oblique shock, $v/U_{1n}=25$	149

List of Figures (cont.)

Figure D.93	δ vs. z/λ_{\parallel} of an oblique shock, $v/U_{1n}=50$	149
Figure D.94	δ vs. z/λ_{\parallel} of an oblique compression region with $b/\lambda_{\parallel} = 0.2$, $v/U_{1n}=25$	150
Figure D.95	δ vs. z/λ_{\parallel} of an oblique compression region with $b/\lambda_{\parallel} = 0.2$, $v/U_{1n}=50$	150
Figure D.96	δ vs. z/λ_{\parallel} of an oblique compression region with $b/\lambda_{\parallel} = 0.5$, $v/U_{1n}=25$	151
Figure D.97	δ vs. z/λ_{\parallel} of an oblique compression region with $b/\lambda_{\parallel} = 0.5$, $v/U_{1n}=50$	151
Figure D.98	δ vs. z/λ_{\parallel} of an oblique compression region with $b/\lambda_{\parallel} = 1.0$, $v/U_{1n}=25$	152
Figure D.99	δ vs. z/λ_{\parallel} of an oblique compression region with $b/\lambda_{\parallel} = 1.0$, $v/U_{1n}=50$	152
Figure D.100	δ vs. z/λ_{\parallel} of an oblique compression region with $b/\lambda_{\parallel} = 2.0$, $v/U_{1n}=25$	153
Figure D.101	δ vs. z/λ_{\parallel} of an oblique compression region with $b/\lambda_{\parallel} = 2.0$, $v/U_{1n}=50$	153
Figure D.102	δ vs. z/λ_{\parallel} of a quasi-parallel shock, $v/U_{1n}=25$	154
Figure D.103	δ vs. z/λ_{\parallel} of a quasi-parallel shock, $v/U_{1n}=50$	154
Figure D.104	δ vs. z/λ_{\parallel} of a quasi-parallel compression region with $b/\lambda_{\parallel} =$ 0.2 , $v/U_{1n}=25$	155
Figure D.105	δ vs. z/λ_{\parallel} of a quasi-parallel compression region with $b/\lambda_{\parallel} =$ 0.2 , $v/U_{1n}=50$	155

List of Figures (cont.)

Figure D.106	δ vs. z/λ_{\parallel} of a quasi-parallel compression region with $b/\lambda_{\parallel} = 0.5$, $v/U_{1n}=25$	156
Figure D.107	δ vs. z/λ_{\parallel} of a quasi-parallel compression region with $b/\lambda_{\parallel} = 0.5$, $v/U_{1n}=50$	156
Figure D.108	δ vs. z/λ_{\parallel} of a quasi-parallel compression region with $b/\lambda_{\parallel} = 1.0$, $v/U_{1n}=25$	157
Figure D.109	δ vs. z/λ_{\parallel} of a quasi-parallel compression region with $b/\lambda_{\parallel} = 1.0$, $v/U_{1n}=50$	157
Figure D.110	δ vs. z/λ_{\parallel} of a quasi-parallel compression region with $b/\lambda_{\parallel} = 2.0$, $v/U_{1n}=25$	158
Figure D.111	δ vs. z/λ_{\parallel} of a quasi-parallel compression region with $b/\lambda_{\parallel} = 2.0$, $v/U_{1n}=50$	158

ศูนย์วิทยทรัพยากร
จุฬาลงกรณ์มหาวิทยาลัย

List of Tables

Table	Page
Table C.1 Simulation parameters for various field angles	97
Table C.2 Simulation parameters for various momenta in the case of a quasi-perpendicular magnetic field.....	98
Table C.3 Simulation parameters for various momenta in the case of an oblique magnetic field	99
Table C.4 Simulation parameters for various momenta in the case of a quasi-parallel magnetic field.....	100
Table D.1 Spectral indices from our simulations with various magnetic field configurations and γ_p values.....	125



 ศูนย์วิทยทรัพยากร
 จุฬาลงกรณ์มหาวิทยาลัย